

Article

A Complex Assemblage of Crystal Habits of Pyrite in the Volcanic Hot Springs from Kamchatka, Russia: Implications for the Mineral Signature of Life on Mars

Min Tang¹ and Yi-Liang Li^{2,*} 

¹ Department of Geology, School of Earth Sciences, Yunnan University, Kunming 650500, China; mtang@ynu.edu.cn

² Department of Earth Sciences, The University of Hong Kong, Hong Kong 999077, China

* Correspondence: yiliang@hku.hk; Tel.: +852-25176912

Received: 30 April 2020; Accepted: 21 June 2020; Published: 23 June 2020



Abstract: In this study, the crystal habits of pyrite in the volcanic hot springs from Kamchatka, Russia were surveyed using scanning electron microscopy. Pyrite crystals occur either as single euhedral crystals or aggregates with a wide range of crystal sizes and morphological features. Single euhedral crystals, with their sizes ranging from ~200 nm to ~40 μm , exhibit combinations of cubic {100}, octahedral {111}, and pyritohedral {210} and {310} forms. Heterogeneous geochemical microenvironments and the bacterial activities in the long-lived hot springs have mediated the development and good preservation of the complex pyrite crystal habits: irregular, spherulitic, cubic, or octahedral crystals congregating with clay minerals, and nanocrystals attaching to the surface of larger pyrite crystals and other minerals. Spherulitic pyrite crystals are commonly covered by organic matter-rich thin films. The coexistence of various sizes and morphological features of those pyrite crystals indicates the results of secular interactions between the continuous supply of energy and nutritional elements by the hot springs and the microbial communities. We suggest that, instead of a single mineral with unique crystal habits, the continuous deposition of the same mineral with a complex set of crystal habits results from the ever-changing physicochemical conditions with contributions from microbial mediation.

Keywords: Kamchatka; hot springs; pyrite; complexity of crystal habits; Mars

1. Introduction

Numerous morphological, molecular, and geochemical biosignatures have been proposed over recent decades in order to identify records of past life in the ‘sedimentary archives’ of the ancient Earth or Mars [1–5]. Among these signatures, a variety of mineralogical biosignatures formed directly or indirectly by bacterial activity provide records of biogenesis in certain environments [6–10]. Microbially-mediated mineral precipitation happens in hot springs because microbial activities may change the concentration of ions in the micro-environments and provide nucleation sites for mineralization. However, the characterization of a biosignature based on the morphology of a single mineral often needs to be used cautiously because of the possibly confusing abiogenic imitators of biosignature [11]. As it is insufficient to take only one single mineral as a biosignature, a suite of parameters that may consistently indicate a biological origin must be considered [1]. It was recently proposed that the synthetic features of a mineral assemblage, including size, crystallinity, and morphology, could be a reference for a specific environment with a certain microbial community. In a study on the diversity of the crystal habits of gypsum, Tang et al. [12] described various morphologies and sizes of gypsum that uniquely coexisted in a square-meter sized volcanic hot spring on the

Kamchatka Peninsula of Russia, and suggested that it was mainly due to the secular interactions between microbial metabolism and geochemical environments. Pyrite is also one of the most common biogenic minerals that are observed as euhedral or framboidal crystals in sediments or sedimentary rocks [8,13]. Laboratory studies of the crystallization of pyrite take physicochemical parameters, such as temperature, pressure, and ion concentrations into consideration and have established the relationship between morphologies of pyrite crystals and their depositional environments [14–21]. Though the chemical pathway of pyrite formation is still in a debate [14,22,23], the direct and indirect effects of biological processes on pyrite crystallization is commonly accepted [20,24]. Microorganisms obtain energy from the geochemical environment and release metabolic products that may affect the chemical composition of their aqueous environments and initiate subsequent mineralization [25–28]. For instance, coupling to the oxidation of organic matter, sulfate-reducing bacteria enzymatically reduce sulfate to hydrogen sulfide, which further reacts with iron in euxinic environments and leads to the precipitation of iron sulfides [29]. Thiel et al. [24] identified a novel type of microbial metabolism that favors energy conservation by oxidizing S^{2-} in FeS to S^- in FeS_2 as a syntrophy coupling to the hydrogenotrophic methanogenesis ($4FeS + 4H_2S + CO_2 \rightarrow 4FeS_2 + CH_4 + 2H_2O$). Microorganisms not only reduce the activation energy barrier for mineral nucleation, but also offer their cell walls as substrates to facilitate the nucleation of crystals [25,30]. Thus, microorganisms are important agents that may induce pyrite mineralization. However, in most cases, it is known that microorganisms have little control over the specific crystal habit of pyrite [26,31]; nevertheless, the biological processes that induce the precipitation of pyrite crystals and/or their assemblages should still carry information about past ecophysiological environments.

Framboid and euhedron are the two dominant morphologies of pyrite crystals in low-temperature sedimentary environments [32,33]. Pyrite is also one of the dominant iron sulfides in natural high-temperature sedimentary environments, such as deep-sea hydrothermal vents and terrestrial hot springs, which are analogs to the early environments for life on Earth [34–36], or possibly early Mars [6]. Pyrite nanoparticles of irregular sizes and shapes in deep-sea hydrothermal vents are considered important sources of iron for the deep ocean biosphere [37,38]. Framboidal and euhedral pyrite crystals were assumed to be generated as a consequence of microbial sulfate-reduction in active shallow submarine vents [39]. Microorganisms also thrive in hot springs that are usually characterized by extreme conditions such as high temperature and low pH through deep geological time [40–43]. Combined with the active iron, the production rate of biogenic hydrogen sulfide influences the amount of iron monosulfide in the system, which may eventually transfer to pyrite [19,24]. Many studies on pyrite in hot spring sediments have focused on the sulfur isotopic signatures (biogenic or abiogenic) [44]. Few data are available on the textures and crystal morphologies of pyrite and the relation to their microbially-mediated environments [45].

Looking for mineral biosignatures in the sedimentary rocks of Earth and Mars has long been an effort because biogenic minerals have a much higher chance of surviving the changing planetary environments during their multi-billion-year of evolution [6,7,46]. For instance, the single domain magnetite of 35–120 nm produced by magnetotactic bacteria has clear protein-modulated mineralization mechanisms and has very well-defined ecophysiological significance [47]. However, a completely inorganic process can also produce single domain magnetite with the same morphology [11]. Textural structures [2,9,48] or the complexity represented by a set of crystal habits, including morphology and size (e.g., gypsum, [12]), were suggested as a new type of biosignature of possible past Martian life. In this paper, we provide a detailed description of the high diversity of mineralogical features of pyrite identified from the Kamchatka volcanic hot springs, which we suggest to be a signature of microbiologically-mediated mineral deposition.

2. Materials and Methods

The Kamchatka Peninsula is located in the transition zone between the Eurasian, North American, and Pacific plates, and is one of the most tectonically active regions on Earth, featuring volcanoes and

earthquakes [49]. There are 31 active volcanoes and hundreds of craters in Kamchatka, but hydrothermal activity is mostly located in the central and eastern volcanic zones [50,51]. As the largest living sulfide ore-forming hydrothermal system in Kamchatka, the Uzon caldera (54°26′–54°31′N, 159°55′–160°07′E) is located in the center of the eastern volcanic zone with thick Paleogene-Neogene sedimentary rocks. It formed after the collapse of the volcanic crater about 40,000 years ago and is underlain by Pliocene volcanogenic sediments [52–54].

Of the hundreds of hot springs in Kamchatka, five were chosen for this study (Figure 1, [55–57]): Burlyashii, Zavarzin, Thermophile, Jen’s Vent, and Oil Pool (Oil Pool lacks data on location and chemistry but is in the same area). Based on geochemical data listed in Table 1, Jen’s Vent and Burlyashii hot springs have the highest temperatures, while Thermophile has the lowest among the hot springs studied. All hot springs are predominantly in reduced geochemical conditions and with pH values varying at large scales (pH = 4.4–7.5). Concentrations of soluble Fe and S²⁻ species of the Burlyashii hot spring are much higher than the other hot springs. The general geochemistry of these volcanic hot springs can be found in Table 1 and Taran [55].

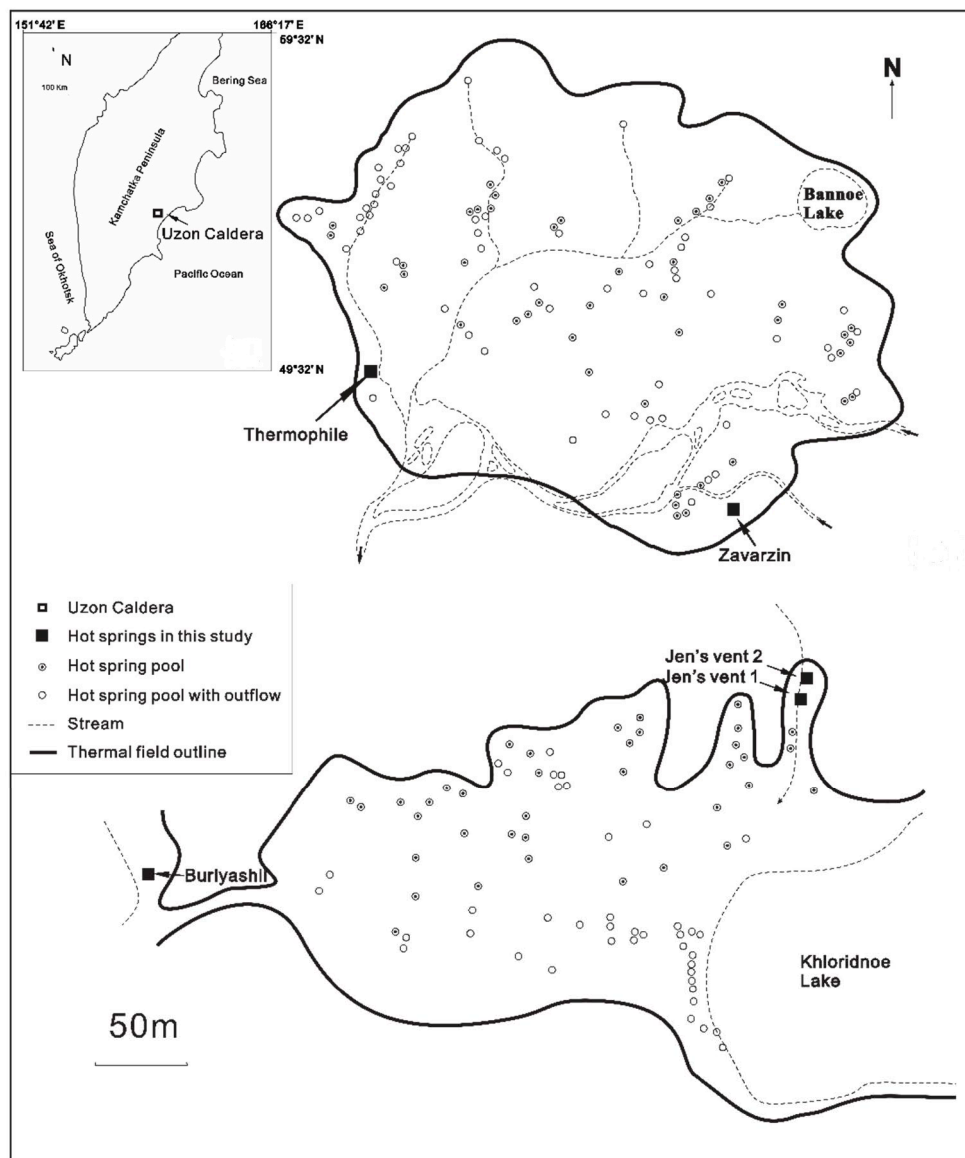


Figure 1. Locations of hot springs in Uzon Caldera, Kamchatka Peninsula (after 56,57).

Table 1. The geochemistry of Kamchatka hot springs. All concentration values are in mmol/l unless otherwise noted.

Parameters	Burlyashii	Zavarzin	Thermophile	Jen's Vent 1	Jen's Vent 2
Temperature (°C)	51–87	54–74	42–70	83	85
Eh (mV)	–90	–96		–240	–240
pH	6–6.5	5.5–7.5	4.4–7	5.3–5.9	5.3–5.9
Alkalinity	1.18–1.23			2.2	0.16–0.18
Soluble Fe	3.75×10^{-3}			0.18×10^{-3}	0.54×10^{-3}
SO ₄ ²⁻	0.23–2.3	0.335–0.557	0.1–0.3	1.35–1.96	1.29–3.125
S ²⁻	$(6.3–43.8) \times 10^{-3}$		$(0.6–43.1) \times 10^{-3}$		
NO ₃ ⁻		0.5		0.063	0.011
NO ₂ ⁻	$(0.1–0.3) \times 10^{-3}$		$(0.2–0.6) \times 10^{-3}$	0.41×10^{-3}	0.54×10^{-3}
NH ₄ ⁺	1.1–1.5	0.84	0.2–4		
References	[58–60]	[57–59,61–63]	[57,58,60]	[64,65]	[64,65]

Samples were collected with sterilized bottles by researchers from the University of Georgia [56], transported to the University of Hong Kong with dry ice, and stored at -21 °C. For scanning electron microscope (SEM) measurements, samples were dehydrated with anhydrous ethanol several times and spread onto silicon chips. The silicon chips were sputtered with gold/palladium for 20 seconds for electron microscopic observation. A Hitachi S4800 SEM in the Electron Microscope Center of the University of Hong Kong was used for morphological and structural characterizations using the secondary electron mode at low voltage (5 kV). Equipped energy-dispersive X-ray spectroscopy (EDS) was used to measure the in-situ chemical composition of each sample to identify minerals based on the primary results of SEM observations.

For Mössbauer spectroscopic measurements, samples were ground to a 200-mesh powder using agate mortar after being freeze-dried. Each sample was mounted onto an acrylic holder (10 mm^2) with a 5 mg Fe/cm^2 thickness. The ⁵⁷Fe Mössbauer spectra were collected at room temperature (293 K) in transmission mode with a 25mCi ⁵⁷Co/Pb source at the University of Hong Kong. The Mössbauer spectroscopic hyperfine parameters were calibrated by the fitted hyperfine parameters of the spectrum of a 25- μm α -Fe film measured after every a few samples.

3. Results and Discussion

The Mössbauer spectra of Oil Pool and Jen's Vent 1 hot spring sediments are shown in Figure 2 and the fitting results are listed in Table 2. Samples from Jen's Vent 1 showed two fitted doublets with chemical isomer shifts (IS) of 0.30 mm/s and 1.06 mm/s, and quadrupole splitting (QS) of 0.60 mm/s and 1.99 mm/s, respectively. The doublet with small IS and QS values was assigned to low-spin Fe²⁺ in pyrite [66], while that with large IS and QS values was assigned to high-spin Fe²⁺ on the lattice of clay minerals. Although Fe²⁺ in pyrite has similar hyperfine parameters to those of Fe³⁺ on the lattice of ferric iron oxides, detailed SEM observations and previous geochemical measurements (Table 1; [41,55]) confirmed the existence of pyrite rather than ferric iron oxides. The parameters in agreement with those of pyrite and Fe²⁺ in silicates [67,68] suggest that iron in Jen's Vent1 mainly existed as Fe²⁺ in pyrite and Fe²⁺-bearing silicates. For the Oil Pool, two doublets with similar parameters were also observed, but showed the high level of Fe²⁺ in pyrite (96.65%).

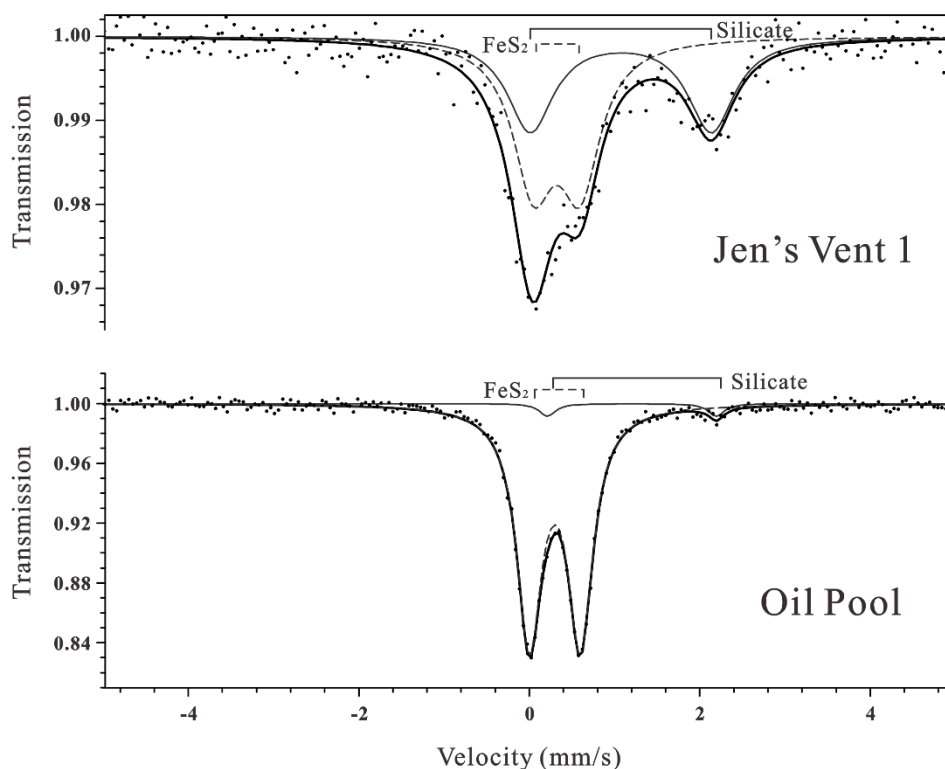


Figure 2. Room temperature ^{57}Fe Mössbauer spectra of low-spin Fe^{2+} in pyrite and high-spin Fe^{2+} on the lattice of silicates (Jen's Vent 1 and Oil Pool).

Table 2. Mössbauer spectroscopic parameters of hot spring sediments.

Sample	Mineral	IS ^a (mm/s)	QS ^b (mm/s)	Area (%)
Jen's Vent 1	FeS_2	0.31	0.55	56.66
	Silicate	1.06	2.13	43.34
Oil Pool	FeS_2	0.30	0.60	96.65
	Silicate	1.22	1.99	3.35

a. IS = isomer shift. b. QS = quadrupole splitting.

Eh-pH diagrams were plotted based on geochemical data of Jen's Vent 1 hot springs (83 °C, activity $[\text{Fe}^{2+}] = 10^{-6.7}$, $[\text{SO}_4^{2-}] = 10^{-2.8}$, according to [65]) which show the thermodynamic stabilities of sulfur species with the current geochemical conditions of these hot springs (Figure 3). It can be seen that the influences of the temperature and ion concentrations on thermodynamic equilibrium in the hot springs studied were insignificant. The electrochemical potentials of Kamchatka hot springs (Table 1) favor the stability of Fe(II) in silicates and pyrite, which is consistent with the Mössbauer spectroscopic results. If only ideal thermodynamic equilibrium is taken into account (Figure 3b), elemental sulfur seems unable to exist in the current springs. However, elemental sulfur was commonly observed in the sediments. The SEM observations showed that some of the elemental sulfur crystals were irregular (Figure 4a) and needed confirmation by EDS analysis (Figure 4b), while others could only be detected based on EDS microanalysis (Figure 4c,d). We also observed a small number of monoclinic sulfur crystals with well-developed crystal faces (Figure 4e) that were chemically confirmed by EDS analysis (Figure 4f). They imply that conditions in favor of sulfur deposition have existed previously.

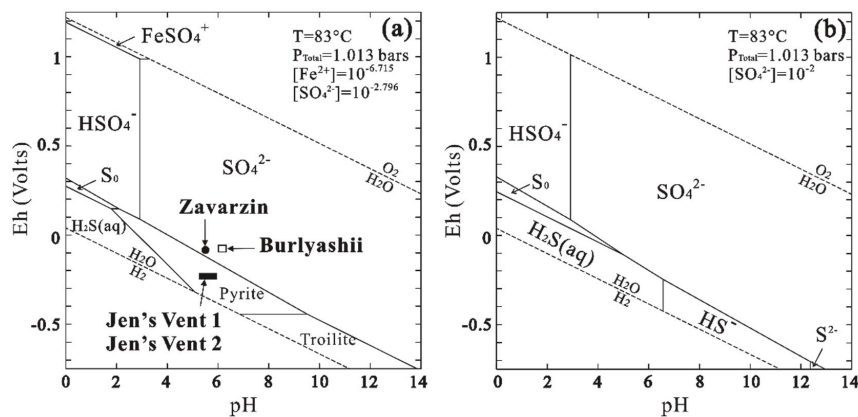


Figure 3. Eh-pH diagrams calculated using Geochemist's Workbench illustrating [69]: (a) Eh, pH, temperature and estimated ion concentrations in Kamchatka hot springs Jen's Vent 1, Vent 2, Zavarzin and Burlyashii (83°C , Activities: $\text{Fe}^{2+} = 10^{-6.715}$, $\text{SO}_4^{2-} = 10^{-2.796}$); (b) The thermodynamic stability of elemental sulfur under the current geochemical conditions (83°C , Activity: $\text{SO}_4^{2-} = 10^{-2}$).

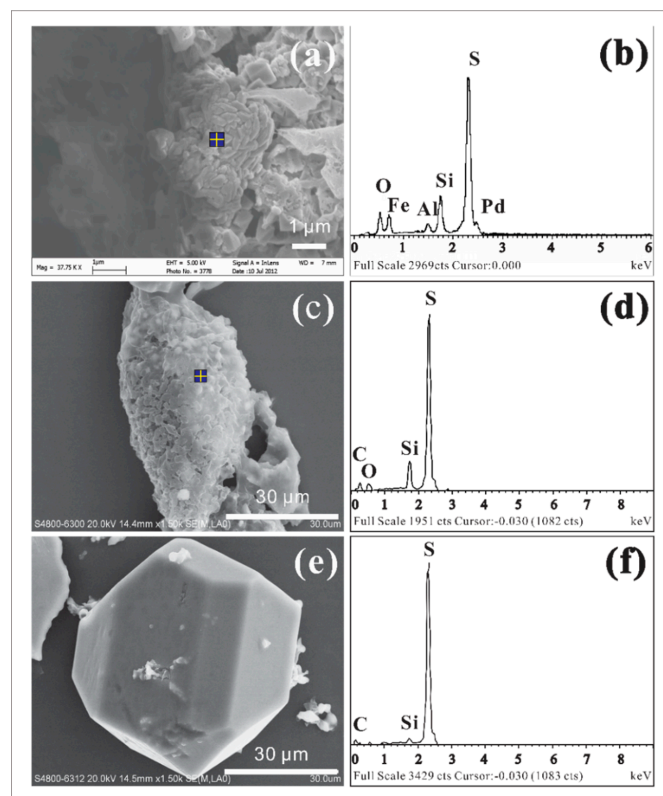


Figure 4. Scanning electron microscope (SEM) images (a,c,e) and energy-dispersive X-ray spectroscopy (EDS)-measured chemical composition of element sulfur (b,d,f) in different morphologies observed in Kamchatka hot springs. The signal of Pd in the spectrum of (b) should be ignored because it was from the instrumental background.

Anaerobic chemoorganoheterotrophic and chemolithoautotrophic bacteria and archaea have been identified and isolated from the Kamchatka hot springs [43,56,70]. Thermophilic sulfate-reducing bacteria (e.g., *Thermoanaerobacterium aciditolerans*), sulfur-reducing bacteria (e.g., *Thermanaerovibrio velox*), sulfur-reducing archaea (e.g., *Thermoproteus uzoniensis*, *Thermoplasmatales*), along with the other thermophilic microorganisms, build up a biological system that interplays with the geochemical system in those hot springs [43,61,71]. Besides those bacterial sulfur redox processes, *Thermoanaerobacter*

ethanolicus and *Carboxydocella manganica* sp. nov. isolated from the hot springs in Kamchatka can reduce Fe(III) for respiration [70,72].

The coexistence of pyrite crystals with a variety of sizes and morphologies were observed and characterized in all the studied hot spring sediments. The size of single euhedral crystals is in a range from ~ 100 nm to ~ 40 μm , with various crystal habits including cubic $\{100\}$, pyritohedral $\{210\}$, octahedral $\{111\}$, pyritohedral $\{310\}$ forms, and their combinations. Irregular or spherical aggregates of pyrite crystals appearing loosely or tightly were also common in the sediments. Most pyrite crystals showed smooth surfaces, while rough surfaces were observed on pyrite covered by clay minerals, organic matter, or the even finer pyrite nanocrystals. However, the framboidal structure of pyrite that is very common in sedimentary rocks and modern marine or lake sediments [19,29,73] was absent in the hot spring sediments. Below are some detailed descriptions of crystal habits.

3.1. Single Crystals

The combination of $a\{100\}$ and $o\{111\}$ forms making cubo-octahedron crystals is the most common combination form of pyrite crystals (Figures 5 and 6a,b). The dominant forms show a trend of transformation between $a\{100\}$ and $o\{111\}$ forms (Figure 5). Such crystals are sometimes elongated cubes because one pair of faces developed to a greater extent (e.g., Figure 5c). The size of single crystals is in a range from ~ 200 nm (Figure 5h) to >40 μm (Figure 5d). Some crystals have smooth surfaces (e.g., Figure 5a), some are covered by clay minerals (e.g., Figure 5d), and others show etched structures on the surface, especially on faces of $o\{111\}$ (e.g., Figure 5c). Sometimes incomplete transformations between two forms result in face going missing during crystal development (Figure 6a,b).

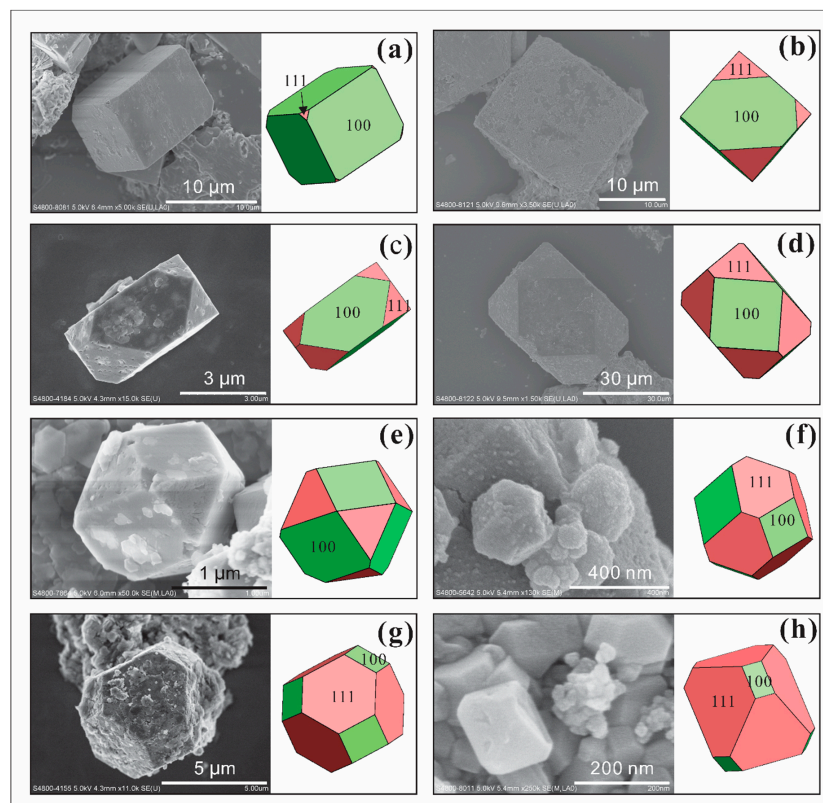


Figure 5. SEM images of single pyrite with combinations of $a\{100\}$ and $o\{111\}$ faces and their corresponding crystal shapes (color drawings on the right), indicating preferential orientation growth in the (100) and (111) directions from (a–h). (a) Pyrite crystals have smooth surfaces. (b,d,g) Pyrite crystals covered by clay minerals. (c,e) Etching pits on the pyrite crystal surface, especially on faces of $o\{111\}$.

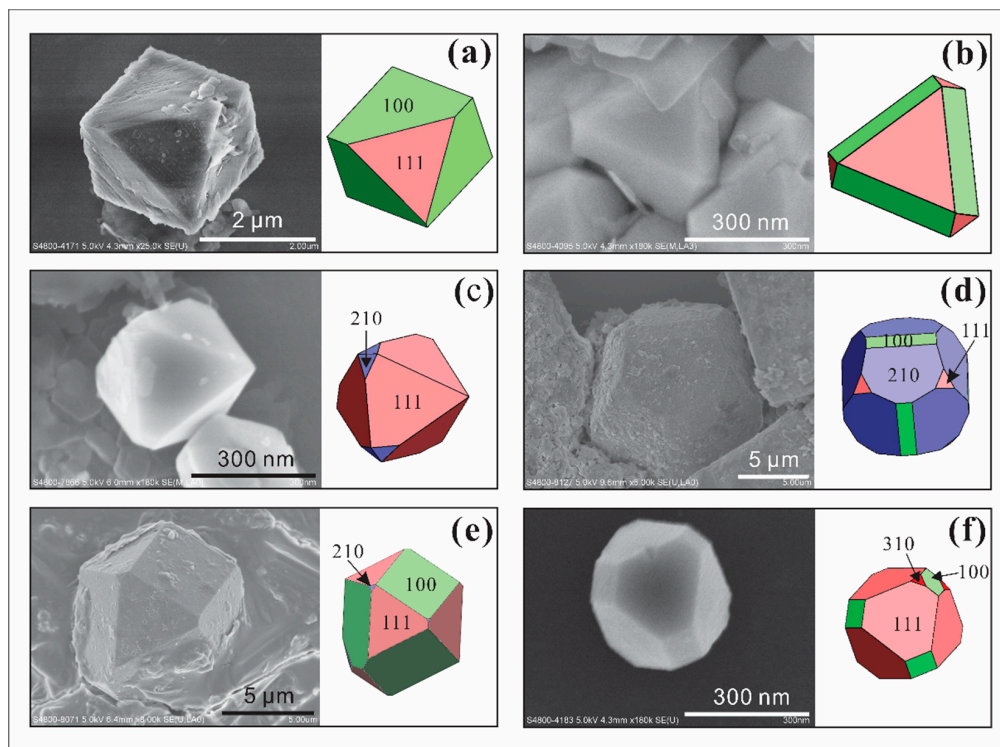


Figure 6. SEM images of single pyrite with combinations of a{100}, o{111}, e{210}, and f{310} faces and their corresponding crystal shapes (color drawings on the right) which show incomplete transformations between two forms result in face going missing during crystal development (a–f).

Combination forms of a{100}, o{111}, e{210}, and f{310} were also observed (Figure 6c–f). The octahedral form is dominant in these crystal habits and shows combinations with the e{210} form (Figure 6c) or with both a{100} and e{210} forms (Figure 6e). The pyritohedral form is dominant in only a few crystals (Figure 6d). A combination of a{100}, o{111}, and f{310} forms in one crystal of pyrite was observed, though the edges were ambiguous owing to its ultrafine size (300 nm, Figure 6f).

3.2. Pyrite Crystal Aggregates

Except those crystals that appeared clearly as single crystals in the sediments, most of them are in the form aggregates. Five types of pyrite crystal aggregates were observed in the spring sediments:

- I pyrite crystals (single crystals with their sizes ranging from 5 to 10 μm) forming aggregates of $\sim 20 \mu\text{m}$ together with clay minerals (Figure 7a,b). The pyrite crystals in these aggregates have combinations of {100}, o{111}, and e{210} habits. This type of aggregate, with sizes ranging from 10 to 100 μm , was commonly found in the samples studied.
- II Parallel intergrowths of pyrite nanocrystals (<300 nm) were observed, which attach to, or nucleate on the o{111} surface of larger pyrite crystals (>10 μm) (Figure 7c,d). The habits of these pyrite nanocrystals are mostly dominated by their o{111} form, which is sometimes slightly modified by e{210}.
- III Pyrite crystal aggregates attaching to the other minerals (Figure 7e,f). They are tiled on the surfaces of the other larger crystals and commonly appear in irregular crystal morphologies. These larger minerals offer surfaces for small pyrite crystals to stick onto.
- IV Massive pyrite nanocrystals (<100 nm) were observed to attach to, or crystallize on the surface of large pyrite crystals (>5 μm) (Figure 8a–g). The habits of these nanocrystals are octahedral (Figure 8d), cubic (Figure 8g), and irregular (Figure 8b). Pyrite nanocrystals do not just attach to or overgrow some surfaces of larger crystals like type II, they also tile the surface. Different stages of pyrite nanocrystal development (irregular crystals with or without obscure edges) are

shown in Figure 8b. Octahedral nanocrystals prefer to attach to $o\{111\}$ faces while cubic ones prefer $a\{100\}$ faces (Figure 8e–g). Some of them grow in a certain direction (Figure 8g).

- V Irregular pyrite nanocrystals aggregate as spherulites (Figure 8e,f,h). Some of the small single aggregates (~ 500 nm) attach to the surfaces of large pyrite crystals (white arrows in Figure 8e,f). Some large aggregates (1–5 μm) attaching to other mineral surfaces are covered by thin films containing organic carbon and sulfur, as measured by EDS (Figure 8h).

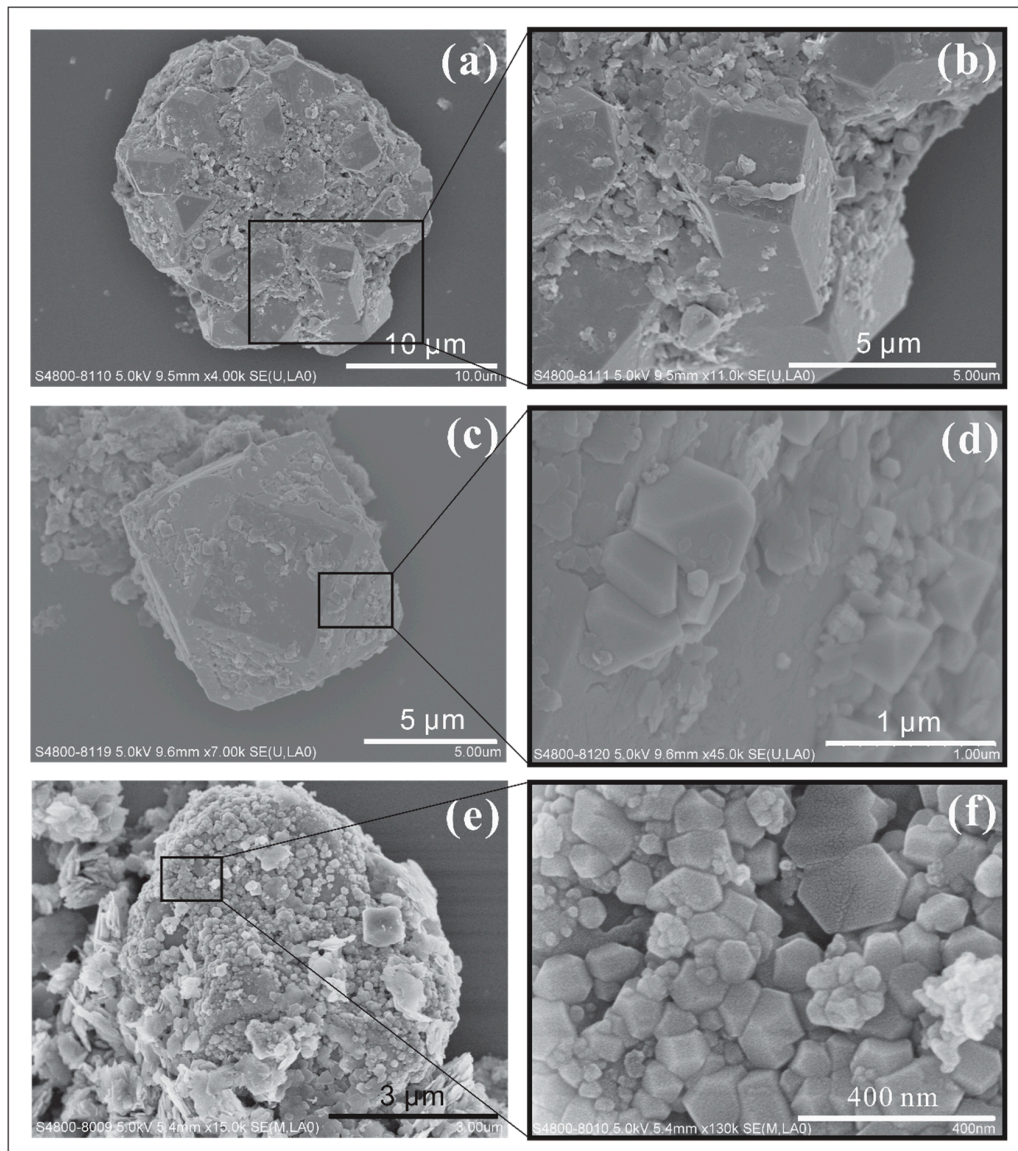


Figure 7. SEM images of pyrite aggregates. (b,d,f) are amplifications of the highlighted areas in images (a,c,e), respectively.

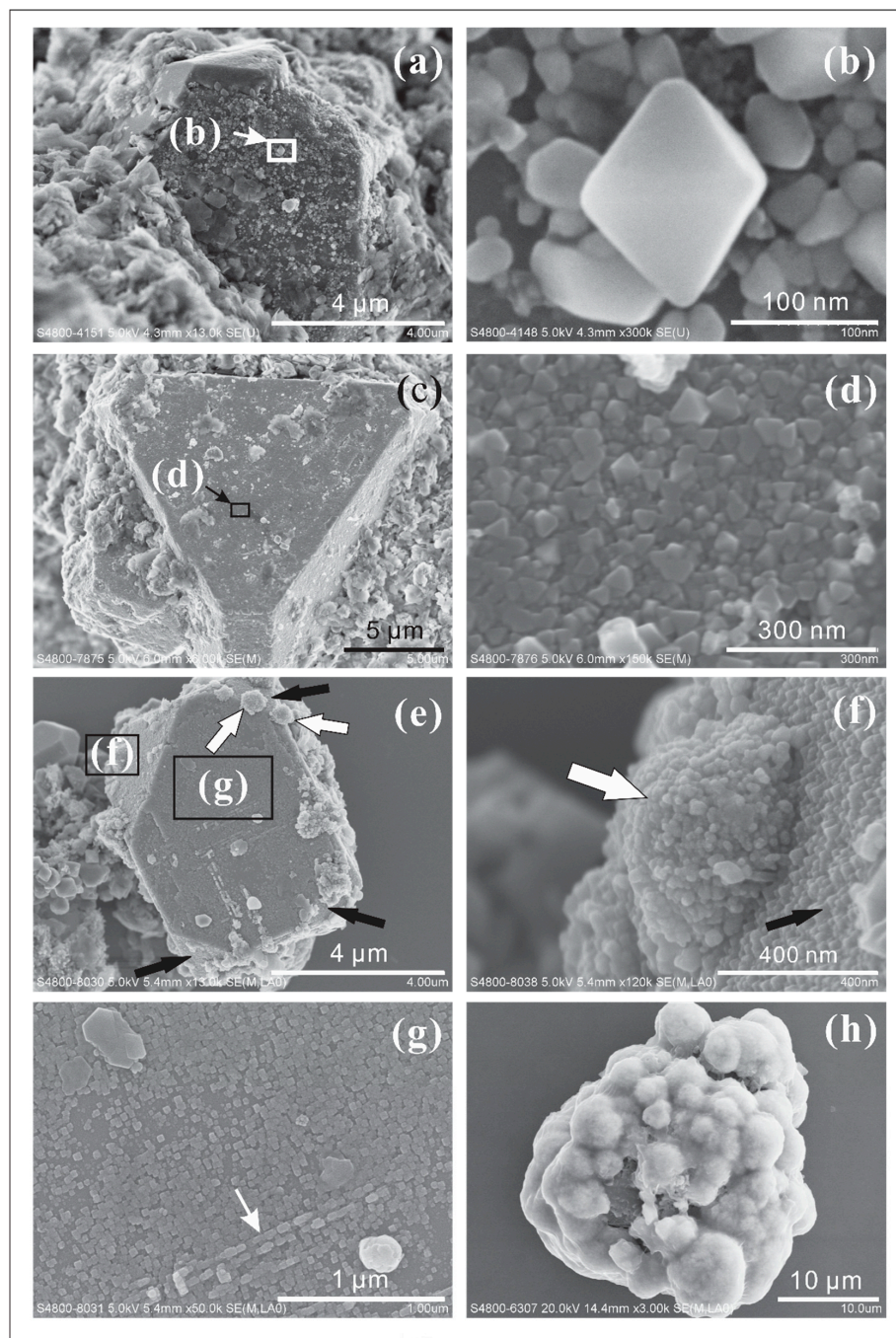


Figure 8. SEM images of pyrite aggregates. **(b)** showed octahedral pyrite crystals highlighted in **(a)**. **(d)** An aggregate of octahedral pyrite crystals on the surface of one bigger crystal in **(c)**. **(f,h)** Irregular pyrite nanocrystals aggregate as spherulites. **(g)** The linear arrangement of pyrite nanocrystals on the surface of a big pyrite crystal **(e)**.

3.3. Intergrowth Texture

Crystal Intergrowths Appear in Four Types:

- I Intergrowth of single crystals. The cubical pyrite intergrowth texture was very common in the hot spring sediments. Cubical pyrite crystals with a size range of 5 to 10 μm show intergrowth with each other, which are sometimes coated by clay minerals (Figure 9a). The octahedral crystals ranging from 300 nm to 1 μm were observed to have intergrowth with each other (Figure 9b) and were covered by thin biofilms, as indicated by EDS measurements.

- II Intergrowth of crystal combinations. Combination crystals of $o\{111\}$ and $a\{100\}$ show intergrowth with each other (Figure 9c). The individual crystals are around $3\ \mu\text{m}$ in size. All faces of $a\{100\}$ form are striated in a specific direction.
- III Twin crystals appear as mirror images across the boundary where each crystal is combined with octahedron and cube habits (Figure 9e). The size of a whole crystal is about $3\ \mu\text{m}$. There are also other small pyrite crystals attached to the edges of twin crystals.
- IV Parallel growth with relative smooth $a\{100\}$ forms and rough $o\{111\}$ forms, which can be covered by a thin layer of clay minerals (Figure 9f). The dimension of a whole crystal is about $700\ \text{nm}$.

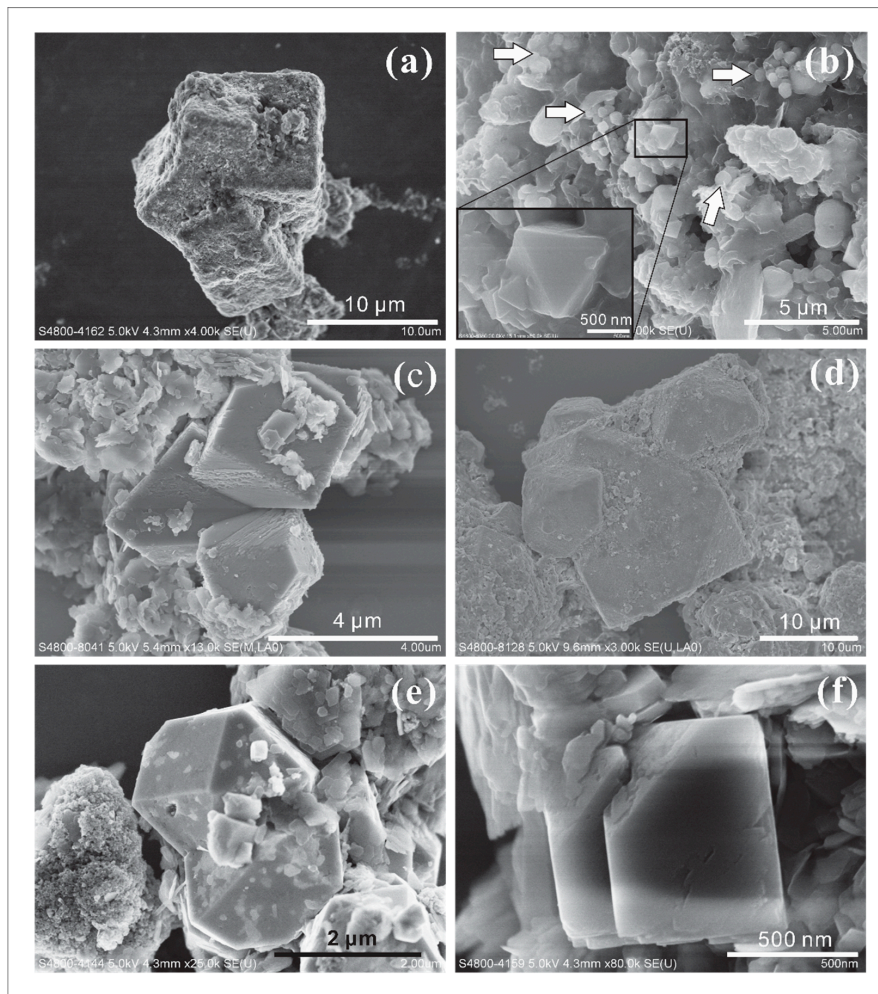


Figure 9. SEM images of different types of intergrowths of pyrite crystals (a–f). The inset at the bottom-left of (b) was the amplification of the highlighted area. (c) Pyrite crystals intergrowth. (e) Pyrite twin crystals. (f) Pyrite crystal parallel growth.

The single forms commonly observed that make pyrite polyhedrons include: cube $a\{100\}$, pyritohedron $e\{210\}$, and octahedron $o\{111\}$ [74]. There are other single forms, such as pyritohedron $f\{310\}$, $\{210\}$, $\{211\}$, $\{321\}$, and a small quantity of $\{221\}$. Combination forms of pyrite crystals were found to be common in these hot spring sediments. As reported in previous studies, cubical pyrite crystals are the most common, while octahedrons are rare among all single forms [75], yet the octahedron form is not rare in the hot spring sediments studied. Normally, the habit of a crystal is confined by the crystallographic structure and defects, and its crystallization environments (mainly temperature and the degree of supersaturation, e.g., [16]). In terrestrial hot springs, the fluctuation of temperature in microenvironments is uncommon, and therefore it has negligible impacts on crystal habits [14].

3.4. Spherulite Pyrite Crystals

Pyrite spherules were observed in sediments of all hot springs (Figure 10). The size of pyrite spherules is usually around 500 nm to 1 μm , aggregated either loosely (Figure 10a) or tightly (Figure 10b). Their assemblages are different from framboidal pyrite, which is made of more euhedral pyrite nanocrystals arranged in a particular order [20]. Framboidal pyrites dominate the crystal forms in black shales (a hydrothermal environment without biologically induced pyrite mineralization, e.g., [76–78]). However, no pyrite framboid was observed in any of the studied hot springs. All of these pyrite spherules are covered by a relatively thick crust of clay rich in organic matter, as indicated by EDS measurements (Figure 10c–f).

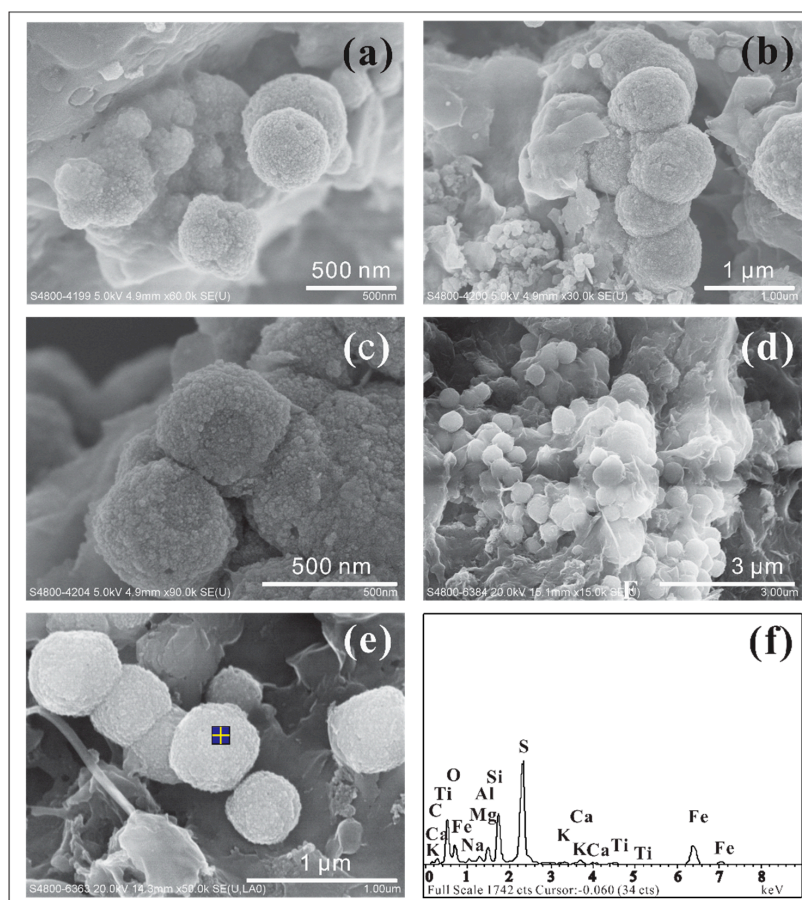


Figure 10. SEM images and the EDS result of spherulitic pyrite crystals that are characterized by biofilm covering materials (a–e), aggregated either loosely (a) or tightly (b). (f) is the EDS profile of the pyrite crystal in (e).

In summary, the diversity of pyrite crystal habits described in this study was found to be much higher than that of authigenic pyrites in deep-sea hydrothermal vents [41,79]. This diversity has been preserved in those small hot springs for >40,000 years [52–54]. The record of the complex crystallographic features over such a long time reflects secular interactions between the continuous supply of energy and nutritional elements by the active hot springs and the metabolisms of the microbial communities.

We can consider a complex assemblage of pyrite forms as the reflection of the interactions between the microbial communities with their geochemical environments, even though there is no direct record of a biologically mediated mineralization. The complex pyrite crystal habits is coincident with the thriving of microbial communities in the Kamchatka volcanic hot springs through time.

Further evaluation of the complexity may develop links between the microbial physiology (e.g., energy metabolism, metal respiration, and nutritional cycles) and the evolution of iron sulfide mineralogy.

This complex set of pyrite crystals may also be a useful reference for the identification of biogenic iron sulfides on Mars. Potential Martian biosignatures using crystal morphology and traits include the deposition of the diagenetic apatite ‘flowers’ as the result of the biological cycle of phosphorus [48], single-domain magnetite formed at low temperatures [80–82], etched pits on the surface of crystals that have cell characteristics [83], abnormally tiny crystal sizes (~2–10 nm) [6,81], unusual crystal lengths in one or more dimensions [84,85], and mineral casts or encrustations preserving biological characteristics [6,85,86]. The formation of a jarosite-goethite-gypsum assemblage was considered to be the result of oxidation of pyrite [87]. The Chemistry and Mineralogy (CheMin) x-ray diffraction (XRD) analyses confirmed the existence of pyrite in mudstone at John Klein by Curiosity rover [88]. However, detailed observations of pyrite crystal on Mars have been limited by in situ measurement methods so far. Some of researchers have tried to look for clues in Martian meteorites. Euhedral pyrite crystals have not often been observed in many meteorites [89,90]. Pyrites in Northwest Africa (NWA) 7533 are cubic or octahedral crystals with average grains sizes of 30–40 μm [91]. Euhedral octahedral pyrite crystals (~50 μm) were observed in Martian meteorite NWA 7475 [92]. These assemblages of pyrite are not as complex as those we observed in the Kamchatka hot springs and their possible hydrothermal genesis [91] may have made the difference. Putative microbial activity in the hot spring environments on Mars in the distant past [93,94] might also have formed similar complex pyrite deposits. Due to the lack of dynamic geological activity and the freezing temperatures on Mars, the microstructures of any complex pyrite deposits in the near-subsurface sediments could be well-preserved for multiple billions of years. However, to fully understand the validity of a well-preserved pyrite complex on Mars, further experiments will be required. Such experiments will need to concentrate on the stability of complex pyrite deposits under various environmental conditions, such as burial, desiccation, heating, and other processes that are likely to have occurred throughout Martian history. Therefore, this presents a new avenue in the search for signs of ancient biota on Mars, and these pyrite complexes should be added to the list of potential signatures of Martian life.

4. Conclusions

The active volcanic hot springs on the Kamchatka Peninsula are extreme environments for microbial ecosystems characterized by the persistent supply of nutrients and geothermal energy. The electron microscopic observations presented in this paper show diverse crystal habits and a wide range of pyrite crystal sizes in the hot springs studied. We propose that it is the continuous interplay between the geochemical environments of the volcanic hot springs and the microbial ecophysiological activities that sustain the continuous precipitation of pyrite and preserve the diverse crystal sizes and habits. We suggest that the complexity of crystal habits of pyrite in those hot springs represents a combined biological and geochemical contribution to the kinetics of pyrite mineralization and its preservation, and thus implies a biologically mediated process.

Author Contributions: Conceptualization, Y.-L.L. and M.T.; methodology, M.T.; validation, Y.-L.L. and M.T.; formal analysis, Y.-L.L. and M.T.; writing—original draft preparation, M.T.; writing—review and editing, Y.-L.L. and M.T.; supervision, Y.-L.L. All authors have read and agreed to the published version of the manuscript.

Funding: This research was funded by RGC, grant number 17312016, NSFC, grant number 31970122 and Joint Foundation Project between Yunnan Science Technology Department and Yunnan University, grant number C176240210019.

Acknowledgments: We thank Juergen Wiegel of the University of Georgia for his generosity in sharing those precious samples.

Conflicts of Interest: The authors declare no conflict of interest.

References

1. Boston, P.; Spilde, M.; Northup, D.; Melim, L.; Soroka, D.; Kleina, L.; Lavoie, K.; Hose, L.; Mallory, L.; Dahm, C. Cave biosignature suites: Microbes, minerals, and Mars. *Astrobiology* **2001**, *1*, 25–55. [[CrossRef](#)] [[PubMed](#)]
2. Douglas, S.; Yang, H. Mineral biosignatures in evaporites: Presence of rosickyite in an endoevaporitic microbial community from Death Valley, California. *Geology* **2002**, *30*, 1075–1078. [[CrossRef](#)]
3. Seager, S.; Turner, E.; Schafer, J.; Ford, E. Vegetation's red edge: A possible spectroscopic biosignature of extraterrestrial plants. *Astrobiology* **2005**, *5*, 372–390. [[CrossRef](#)] [[PubMed](#)]
4. Chan, C.S.; Fakra, S.; Emerson, D.; Fleming, E.J.; Edwards, K.J. Lithotrophic iron-oxidizing bacteria produce organic stalks to control mineral growth: Implications for biosignature formation. *ISME J.* **2011**, *5*, 717–727. [[CrossRef](#)]
5. Summons, R.E.; Amend, J.P.; Bish, D.; Buick, R.; Cody, G.D.; Des Marais, D.J.; Dromart, G.; Eigenbrode, J.L.; Knoll, A.H.; Sumner, D.Y. Preservation of Martian organic and environmental records: Final report of the Mars Biosignature Working Group. *Astrobiology* **2011**, *11*, 157–181. [[CrossRef](#)]
6. Banfield, J.F.; Moreau, J.W.; Chan, C.S.; Welch, S.A.; Little, B. Mineralogical biosignatures and the search for life on Mars. *Astrobiology* **2001**, *1*, 447–465. [[CrossRef](#)] [[PubMed](#)]
7. Cady, S.L.; Farmer, J.D.; Grotzinger, J.P.; Schopf, J.W.; Steele, A. Morphological biosignatures and the search for life on Mars. *Astrobiology* **2003**, *3*, 351–368. [[CrossRef](#)]
8. Dove, P.M.; De Yoreo, J.J.; Weiner, S. *Bioineralization*; Mineralogical Society of America and the Geochemical Society: Washington, DC, USA, 2003; Volume 54, pp. 10–17.
9. Douglas, S. Microbial biosignatures in evaporite deposits: Evidence from Death Valley, California. *Planet. Space Sci.* **2004**, *52*, 223–227. [[CrossRef](#)]
10. Fortin, D.; Langley, S. Formation and occurrence of biogenic iron-rich minerals. *Earth Sci. Rev.* **2005**, *72*, 1–19. [[CrossRef](#)]
11. Golden, D.C.; Ming, D.W.; Morris, R.V.; Brearley, A.J.; Lauer, H.V.; Treiman, A.H.; Zolensky, M.E.; Schwandt, C.S.; Lofgren, G.E.; McKay, G.A. Evidence for exclusively inorganic formation of magnetite in Martian meteorite ALH84001. *Am. Mineral.* **2004**, *89*, 681–695. [[CrossRef](#)]
12. Tang, M.; Ehreiser, A.; Li, Y.-L. Gypsum in modern Kamchatka volcanic hot springs and the Lower Cambrian black shale: Applied to the microbial-mediated precipitation of sulfates on Mars. *Am. Mineral.* **2014**, *99*, 2126–2137. [[CrossRef](#)]
13. Wilkin, R.T.; Barnes, H.L.; Brantley, S.L. The size distribution of framboidal pyrite in modern sediments: An indicator of redox conditions. *Geochim. Cosmochim. Acta* **1996**, *60*, 3897–3912. [[CrossRef](#)]
14. Xian, H.; Zhu, J.; Liang, X.; He, H. Morphology controllable syntheses of micro- and nano-iron pyrite mono- and poly-crystals: A review. *RSC Adv.* **2016**, *6*, 31988–31999. [[CrossRef](#)]
15. Luther, G.W., III. Pyrite synthesis via polysulfide compounds. *Geochim. Cosmochim. Acta* **1991**, *55*, 2839–2849. [[CrossRef](#)]
16. Morse, J.W.; Wang, Q. Pyrite formation under conditions approximating those in anoxic sediments: II. Influence of precursor iron minerals and organic matter. *Mar. Chem.* **1997**, *57*, 187–193. [[CrossRef](#)]
17. Rickard, D. Kinetics of pyrite formation by the H₂S oxidation of iron (II) monosulfide in aqueous solutions between 25 and 125 °C: The rate equation. *Geochim. Cosmochim. Acta* **1997**, *61*, 115–134. [[CrossRef](#)]
18. Rickard, D.; Luther, G.W., III. Kinetics of pyrite formation by the H₂S oxidation of iron (II) monosulfide in aqueous solutions between 25 and 125 °C: The mechanism. *Geochim. Cosmochim. Acta* **1997**, *61*, 135–147. [[CrossRef](#)]
19. Schoonen, M.A. Mechanisms of sedimentary pyrite formation. In *Sulfur Biogeochemistry—Past and Present*; Amend, J.P., Edwards, K.J., Lyons, T.W., Eds.; The Geological Society of America, Inc.: Boulder, CO, USA, 2004; pp. 117–134.
20. Ohfuji, H.; Rickard, D. Experimental syntheses of framboids—A review. *Earth Sci. Rev.* **2005**, *71*, 147–170. [[CrossRef](#)]
21. Wang, D.; Wang, Q.; Wang, T. Shape controlled growth of pyrite FeS₂ crystallites via a polymer-assisted hydrothermal route. *CrystEngComm* **2010**, *12*, 3797–3805. [[CrossRef](#)]
22. Goldhaber, M.B. Sulfur-rich sediments. In *Treatise on Geochemistry*; Holland, H.D., Turekian, K.K., Eds.; Pergamon: Oxford, UK, 2003; Volume 7, pp. 257–288.

23. Rickard, D.; Luther, G.W., III. Chemistry of iron sulfides. *Chem. Rev.* **2007**, *107*, 514–562. [[CrossRef](#)] [[PubMed](#)]
24. Thiel, J.; Byrne, J.M.; Kappler, A.; Schink, B.; Pester, M. Pyrite formation from FeS and H₂S is mediated by a novel type of microbial energy metabolism. *bioRxiv* **2018**, 396978. [[CrossRef](#)]
25. Fortin, D.; Beveridge, T.J. Microbial sulfate reduction within sulfidic mine tailings: Formation of diagenetic Fe sulfides. *Geomicrobiol. J.* **1997**, *14*, 1–21. [[CrossRef](#)]
26. Konhauser, K.O. Diversity of bacterial iron mineralization. *Earth Sci. Rev.* **1998**, *43*, 91–121. [[CrossRef](#)]
27. Baeuerlein, E. *Bio-mineralization: From Biology to Biotechnology and Medical Application*; Wiley-VCH: Weinheim, Germany, 2004; pp. 159–176.
28. Panda, A.K.; Bisht, S.S.; De Mandal, S.; Kumar, N.S. Bacterial and archeal community composition in hot springs from Indo-Burma region, North-east India. *AMB Express* **2016**, *6*. [[CrossRef](#)] [[PubMed](#)]
29. Berner, R.A. Sedimentary pyrite formation: An update. *Geochim. Cosmochim. Acta* **1984**, *48*, 605–615. [[CrossRef](#)]
30. Severmann, S.; Mills, R.A.; Palmer, M.R.; Telling, J.P.; Cragg, B.; John Parkes, R. The role of prokaryotes in subsurface weathering of hydrothermal sediments: A combined geochemical and microbiological investigation. *Geochim. Cosmochim. Acta* **2006**, *70*, 1677–1694. [[CrossRef](#)]
31. Weiner, S.; Dove, P.M. An overview of biomineralization processes and the problem of the vital effect. In *Bio-mineralization*; Dove, P.M., De Yoreo, J.J., Weiner, S., Eds.; Mineralogical Society of America and Geochemical Society: Washington, DC, USA, 2003; Volume 54, pp. 1–29.
32. Sweeney, R.E.; Kaplan, I.R. Pyrite framboid formation: Laboratory synthesis and marine sediments. *Econ. Geol.* **1973**, *68*, 618–634. [[CrossRef](#)]
33. Maclean, L.C.W.; Tyliszczak, T.; Gilbert, P.U.P.A.; Zhou, D.; Pray, T.J.; Onstott, T.C.; Southam, G. A high-resolution chemical and structural study of framboidal pyrite formed within a low-temperature bacterial biofilm. *Geobiology* **2008**, *6*, 471–480. [[CrossRef](#)] [[PubMed](#)]
34. Haymon, R.M.; Kastner, M. Hot spring deposits on the east pacific rise at 21° N: Preliminary description of mineralogy and genesis. *Earth Planet. Sci. Lett.* **1981**, *53*, 363–381. [[CrossRef](#)]
35. Vargas, M.; Kashefi, K.; Blunt-Harris, E.L.; Lovley, D.R. Microbiological evidence for Fe(III) reduction on early Earth. *Nature* **1998**, *395*, 65–67. [[CrossRef](#)] [[PubMed](#)]
36. Westall, F. Early life on earth and analogies to mars. In *Water on Mars and Life*; Tokano, T., Ed.; Springer: Berlin/Heidelberg, Germany, 2005; Volume 4, pp. 45–64.
37. Yücel, M.; Gartman, A.; Chan, C.S.; Luther, G.W., III. Hydrothermal vents as a kinetically stable source of iron-sulphide-bearing nanoparticles to the ocean. *Nat. Geosci.* **2011**, *4*, 367–371. [[CrossRef](#)]
38. Gartman, A.; Luther, G.W., III. Comparison of pyrite (FeS₂) synthesis mechanisms to reproduce natural FeS₂ nanoparticles found at hydrothermal vents. *Geochim. Cosmochim. Acta* **2013**, *120*, 447–458. [[CrossRef](#)]
39. Prol-Ledesma, R.M.; Canet, C.; Villanueva-Estrada, R.E.; Ortega-Osorio, A. Morphology of pyrite in particulate matter from shallow submarine hydrothermal vents. *Am. Mineral.* **2010**, *95*, 1500–1507. [[CrossRef](#)]
40. Barghoorn, E.S.; Nichols, R.L. Sulfate-reducing bacteria and pyritic sediments in Antarctica. *Science* **1961**, *134*, 190. [[CrossRef](#)] [[PubMed](#)]
41. Schieber, J. Sedimentary pyrite: A window into the microbial past. *Geology* **2002**, *30*, 531–534. [[CrossRef](#)]
42. Elshahed, M.S.; Senko, J.M.; Najar, F.Z.; Kenton, S.M.; Roe, B.A.; Dewers, T.A.; Spear, J.R.; Krumholz, L.R. Bacterial diversity and sulfur cycling in a mesophilic sulfide-rich spring. *Appl. Environ. Microbiol.* **2003**, *69*, 5609–5621. [[CrossRef](#)] [[PubMed](#)]
43. Wagner, I.D.; Wiegel, J. Diversity of thermophilic anaerobes. *Ann. N. Y. Acad. Sci.* **2008**, *1125*, 1–43. [[CrossRef](#)]
44. Rice, C.; Ashcroft, W.; Batten, D.; Boyce, A.; Caulfield, J.; Fallick, A.; Hole, M.; Jones, E.; Pearson, M.; Rogers, G. A Devonian auriferous hot spring system, Rhynie, Scotland. *J. Geol. Soc. Lond.* **1995**, *152*, 229–250. [[CrossRef](#)]
45. Westall, F.; de Wit, M.J.; Dann, J.; van der Gaast, S.; de Ronde, C.E.J.; Gerneke, D. Early Archean fossil bacteria and biofilms in hydrothermally-influenced sediments from the Barberton greenstone belt, South Africa. *Precambrian Res.* **2001**, *106*, 93–116. [[CrossRef](#)]
46. Westall, F. Morphological biosignatures in early terrestrial and extraterrestrial materials. In *Strategies of Life Detection*; Botta, O., Bada, J.L., Gomez-Elvira, J., Javaux, E., Selsis, F., Summons, R., Eds.; Springer: Boston, MA, USA, 2008; pp. 95–114.
47. Bazylinski, D.; Frankel, R. Magnetosome formation in prokaryotes. *Nat. Rev. Microbiol.* **2004**, *2*, 217–230. [[CrossRef](#)]

48. Sun, S.; Chan, L.; Li, Y.-L. What lurks in the Martian rocks and soil? Investigations of sulfates, phosphates, and perchlorates. Flower-like apatite recording microbial processes through deep geological time and its implication to the search for mineral records of life on Mars. *Am. Mineral.* **2014**, *99*, 2116–2125. [[CrossRef](#)]
49. Gorbатов, A.; Kostoglodov, V.; Suarez, G.; Gordeev, E. Seismicity and structure of the Kamchatka subduction zone. *J. Geophys. Res. Solid Earth* **1997**, *102*, 17883–17898. [[CrossRef](#)]
50. Okrugin, V.M.; Tazaki, K.; Bel'kova, N.L. Hydrothermal mineral formation systems of Kamchatka and the biomineralization. In *Proceedings: International Symposium of the Kanazawa University 21st-Century COE Program*; Kamta, N., Ed.; Kanazawa University: Kanazawa, Japan, 2003; Volume 1, pp. 235–238.
51. Kozhurin, A.; Acocella, V.; Kyle, P.R.; Lagmay, F.M.; Melekestsev, I.V.; Ponomareva, V.; Rust, D.; Tibaldi, A.; Tunesi, A.; Corazzato, C.; et al. Trenching studies of active faults in Kamchatka, eastern Russia: Palaeoseismic, tectonic and hazard implications. *Tectonophysics* **2006**, *417*, 285–304. [[CrossRef](#)]
52. Karpov, G.A.; Naboko, S.I. Metal contents of recent thermal waters, mineral precipitates and hydrothermal alteration in active geothermal fields, Kamchatka. *J. Geochem. Explor.* **1990**, *36*, 57–71. [[CrossRef](#)]
53. Waltham, T. A guide to the volcanoes of southern Kamchatka, Russia. *Proc. Geol. Assoc.* **2001**, *112*, 67–78. [[CrossRef](#)]
54. Kontorovich, A.E.; Bortnikova, S.B.; Karpov, G.A.; Kashirtsev, V.A.; Kostyreva, E.A.; Fomin, A.N. Uzon volcano caldera (Kamchatka): A unique natural laboratory of the present-day naphthide genesis. *Russ. Geol. Geophys.* **2011**, *52*, 768–772. [[CrossRef](#)]
55. Taran, Y. Geochemistry of volcanic and hydrothermal fluids and volatile budget of the Kamchatka–Kuril subduction zone. *Geochim. Cosmochim. Acta* **2009**, *73*, 1067–1094. [[CrossRef](#)]
56. Zhao, W. Diversity and Potential Geochemical Functions of Prokaryotes in Hot Springs of the Uzon Caldera, Kamchatka. Ph.D. Thesis, The University of Georgia, Athens, GA, USA, 2008.
57. Hollingsworth, E.R. Elemental and Isotopic Chemistry of the Uzon Caldera: The Evolution of Thermal Waters, Gas, and Mineral Precipitation. Master's Thesis, The University of Georgia, Athens, GA, USA, 2006.
58. Goin, J.C.; Cady, S.L. Biosedimentological processes that produce hot spring sinter biofabrics: Examples from the Uzon Caldera, Kamchatka Russia. In *From Fossils to Astrobiology*; Seckbach, J., Walsh, M., Eds.; Springer: Dordrecht, The Netherlands, 2009; Volume 12, pp. 159–179.
59. Kochetkova, T.; Rusanov, I.; Pimenov, N.; Kolganova, T.; Lebedinsky, A.; Bonch-Osmolovskaya, E.; Sokolova, T. Anaerobic transformation of carbon monoxide by microbial communities of Kamchatka hot springs. *Extremophiles* **2011**, *15*, 319–325. [[CrossRef](#)]
60. Zhao, W.; Song, Z.; Jiang, H.; Li, W.; Mou, X.; Romanek, C.S.; Wiegel, J.; Dong, H.; Zhang, C.L. Ammonia-oxidizing Archaea in Kamchatka Hot Springs. *Geomicrobiol. J.* **2011**, *28*, 149–159. [[CrossRef](#)]
61. Burgess, E.A. Geomicrobiological Description of Two Contemporary Hydrothermal Pools in Uzon Caldera, Kamchatka, Russia, as Models for Sulfur Biogeochemistry. Ph.D. Thesis, The University of Georgia, Athens, GA, USA, 2009.
62. Burgess, E.; Unrine, J.; Mills, G.; Romanek, C.; Wiegel, J. Comparative geochemical and microbiological characterization of two thermal pools in the Uzon Caldera, Kamchatka, Russia. *Microb. Ecol.* **2012**, *63*, 471–489. [[CrossRef](#)] [[PubMed](#)]
63. Gumerov, V.M.; Mardanov, A.V.; Beletsky, A.V.; Prokofeva, M.I.; Bonch-Osmolovskaya, E.A.; Ravin, N.V.; Skryabin, K.G. Complete genome sequence of “*Vulcanisaeta moutnovskia*” strain 768-28, a novel member of the hyperthermophilic crenarchaeal genus *Vulcanisaeta*. *J. Bacteriol.* **2011**, *193*, 2355–2356. [[CrossRef](#)] [[PubMed](#)]
64. Kyle, J.E. Mineral-Microbe Interactions and Biomineralization of Siliceous Sinters and Underlying Rock from Jenn's Pools in the Uzon Caldera, Kamchatka, Russia. Master's Thesis, The University of Georgia, Athens, GA, USA, 2005.
65. Kyle, J.E.; Schroeder, P.A.; Wiegel, J. Microbial silicification in sinters from two terrestrial hot springs in the Uzon Caldera, Kamchatka, Russia. *Geomicrobiol. J.* **2007**, *24*, 627–641. [[CrossRef](#)]
66. McCammon, C. Mössbauer spectroscopy of minerals. In *Mineral Physics and Crystallography: A Handbook of Physical Constants*; Ahrens, T.J., Ed.; American Geophysical Union: Washington, DC, USA, 1995; Volume 2, pp. 332–347.
67. Evans, B.J.; Johnson, R.G.; Senftle, F.E.; Cecil, C.B.; Dulong, F. The ⁵⁷Fe Mössbauer parameters of pyrite and marcasite with different provenances. *Geochim. Cosmochim. Acta* **1982**, *46*, 761–775. [[CrossRef](#)]
68. Dyar, M.D.; Agresti, D.G.; Schaefer, M.W.; Grant, C.A.; Sklute, E.C. Mössbauer spectroscopy of earth and planetary materials. *Annu. Rev. Earth Planet. Sci.* **2006**, *34*, 83–125. [[CrossRef](#)]

69. Bethke, C.M.; Yeakel, S. *The Geochemist's Workbench, Release 7.0: GWB Essentials Guide*; Hydrogeology Program; University of Illinois: Urbana, IL, USA, 2007; pp. 1–98.
70. Kublanov, I.V.; Perevalova, A.A.; Slobodkina, G.B.; Lebedinsky, A.V.; Bidzhieva, S.K.; Kolganova, T.V.; Kaliberda, E.N.; Rumsh, L.D.; Haertlé, T.; Bonch-Osmolovskaya, E.A. Biodiversity of thermophilic prokaryotes with hydrolytic activities in hot springs of Uzon Caldera, Kamchatka (Russia). *Appl. Environ. Microbiol.* **2009**, *75*, 286–291. [[CrossRef](#)]
71. Mardanov, A.V.; Gumerov, V.M.; Beletsky, A.V.; Perevalova, A.A.; Karpov, G.A.; Bonch-Osmolovskaya, E.A.; Ravin, N.V. Uncultured archaea dominate in the thermal groundwater of Uzon Caldera, Kamchatka. *Extremophiles* **2011**, *15*, 365–372. [[CrossRef](#)]
72. Slobodkina, G.B.; Panteleeva, A.N.; Sokolova, T.G.; Bonch-Osmolovskaya, E.A.; Slobodkin, A.I. Carboxydocella manganica sp nov., a thermophilic, dissimilatory Mn(IV)- and Fe(III)-reducing bacterium from a Kamchatka hot spring. *Int. J. Syst. Evol. Microbiol.* **2012**, *62*, 890–894. [[CrossRef](#)]
73. Wilkin, R.T.; Barnes, H.L. Pyrite formation in an anoxic estuarine basin. *Am. J. Sci.* **1997**, *297*, 620–650. [[CrossRef](#)]
74. Anthony, J.W.; Bideaux, R.A.; Bladh, K.W.; Nichols, M.C. *Handbook of Mineralogy*; Mineralogical Society of America: Chantilly, CA, USA, 2005; p. 4129.
75. Blackburn, W.H.; Dennen, W.H. *Principles of Mineralogy*; William C Brown Pub: Dubuque, IA, USA, 1994; p. 413.
76. Steiner, M.; Wallis, E.; Erdtmann, B.-D.; Zhao, Y.; Yang, R. Submarine-hydrothermal exhalative ore layers in black shales from South China and associated fossils—Insights into a lower Cambrian facies and bio-evolution. *Palaeogeogr. Palaeoclim. Palaeoecol.* **2001**, *169*, 165–191. [[CrossRef](#)]
77. Jiang, S.-Y.; Chen, Y.-Q.; Ling, H.-F.; Yang, J.-H.; Feng, H.-Z.; Ni, P. Trace- and rare-earth element geochemistry and Pb–Pb dating of black shales and intercalated Ni–Mo–PGE–Au sulfide ores in Lower Cambrian strata, Yangtze Platform, South China. *Min. Depos.* **2006**, *41*, 453–467. [[CrossRef](#)]
78. Xu, J.; Li, Y.-L. An SEM study of microfossils in the black shale of the lower Cambrian niutitang formation, southwest China: Implications for the polymetallic sulfide mineralization. *Ore Geol. Rev.* **2015**, *65*, 811–820. [[CrossRef](#)]
79. Juniper, S.K.; Thompson, J.A.J.; Calvert, S.E. Accumulation of minerals and trace elements in biogenic mucus at hydrothermal vents. *Deep Sea Res. Part A Oceanogr. Res. Pap.* **1986**, *33*, 339–347. [[CrossRef](#)]
80. Thomas-Keprta, K.L.; Bazylinski, D.A.; Kirschvink, J.L.; Clemett, S.J.; McKay, D.S.; Wentworth, S.J.; Vali, H.; Gibson, E.K., Jr.; Romanek, C.S. Elongated prismatic magnetite crystals in ALH84001 carbonate globules: Potential Martian magnetofossils. *Geochim. Cosmochim. Acta* **2000**, *64*, 4049–4081. [[CrossRef](#)]
81. Thomas-Keprta, K.L.; Clemett, S.J.; Bazylinski, D.A.; Kirschvink, J.L.; McKay, D.S.; Wentworth, S.J.; Vali, H.; Gibson, E.K.; McKay, M.F.; Romanek, C.S. Truncated hexa-octahedral magnetite crystals in ALH84001: Presumptive biosignatures. *Proc. Natl. Acad. Sci. USA* **2001**, *98*, 2164–2169. [[CrossRef](#)] [[PubMed](#)]
82. Thomas-Keprta, K.L.; Clemett, S.J.; Bazylinski, D.A.; Kirschvink, J.L.; McKay, D.S.; Wentworth, S.J.; Vali, H.; Gibson, E.K., Jr.; Romanek, C.S. Magnetofossils from ancient Mars: A robust biosignature in the Martian meteorite ALH84001. *Appl. Environ. Microbiol.* **2002**, *68*, 3663–3672. [[CrossRef](#)]
83. Fisk, M.R.; Giovannoni, S.J.; Thorseth, I.H. Alteration of oceanic volcanic glass: Textural evidence of microbial activity. *Science* **1998**, *281*, 978–980. [[CrossRef](#)]
84. MacLachlan, M.; Manners, I.; Ozin, G.A. New (inter)faces: Polymers and inorganic materials. *Adv. Mater.* **2000**, *12*, 675–681. [[CrossRef](#)]
85. Barbieri, R.; Stivaletta, N.; Marinangeli, L.; Ori, G.-G. Microbial signatures in sabkha evaporite deposits of Chott el Gharsa (Tunisia) and their astrobiological implications. *Planet. Space Sci.* **2006**, *54*, 726–736. [[CrossRef](#)]
86. Hofmann, B.; Farmer, J. Filamentous fabrics in low-temperature mineral assemblages: Are they fossil biomarkers? Implications for the search for a subsurface fossil record on the early Earth and Mars. *Planet. Space Sci.* **2000**, *48*, 1077–1086. [[CrossRef](#)]
87. Zolotov, M.Y.; Shock, E.L. Formation of jarosite-bearing deposits through aqueous oxidation of pyrite at meridiani planum, mars. *Geophys. Res. Lett.* **2005**, *32*, L21203. [[CrossRef](#)]
88. Vaniman, D.T.; Bish, D.L.; Ming, D.W.; Bristow, T.F.; Morris, R.V.; Blake, D.F.; Chipera, S.J.; Morrison, S.M.; Treiman, A.H.; Rampe, E.B.; et al. Mineralogy of a mudstone at Yellowknife Bay, Gale crater, Mars. *Science* **2014**, *343*, 1243480. [[CrossRef](#)] [[PubMed](#)]

89. Greenwood, J.P.; Mojzsis, S.J.; Coath, C.D. Sulfur isotopic compositions of individual sulfides in Martian meteorites ALH84001 and Nakhla: Implications for crust–regolith exchange on Mars. *Earth Planet. Sci. Lett.* **2000**, *184*, 23–35. [[CrossRef](#)]
90. Lorand, J.-P.; Pont, S.; Chevrier, V.; Luguët, A.; Zanda, B.; Hewins, R. Petrogenesis of Martian sulfides in the chassigny meteorite. *Am. Mineral.* **2018**, *103*, 872–885. [[CrossRef](#)]
91. Lorand, J.-P.; Hewins, R.; Remusat, L.; Zanda, B.; Pont, S.; Leroux, H.; Marinova, M.; Jacob, D.; Humayun, M.; Nemchin, A.; et al. Nickeliferous pyrite tracks pervasive hydrothermal alteration in Martian regolith breccia: A study in nwa 7533. *Meteorit. Planet. Sci.* **2015**, *50*, 2099–2120. [[CrossRef](#)]
92. Wittmann, A.; Korotev, R.L.; Jolliff, B.L.; Irving, A.J.; Moser, D.E.; Barker, I.; Rumble, D., III. Petrography and composition of Martian regolith breccia meteorite northwest Africa 7475. *Meteorit. Planet. Sci.* **2015**, *50*, 326–352. [[CrossRef](#)]
93. Boston, P.; Ivanov, M.; McKay, C. On the possibility of chemosynthetic ecosystems in subsurface habitats on Mars. *Icarus* **1992**, *95*, 300–308. [[CrossRef](#)]
94. Allen, C.C.; Oehler, D.Z. A case for ancient springs in Arabia Terra, Mars. *Astrobiology* **2008**, *8*, 1093–1112. [[CrossRef](#)]



© 2020 by the authors. Licensee MDPI, Basel, Switzerland. This article is an open access article distributed under the terms and conditions of the Creative Commons Attribution (CC BY) license (<http://creativecommons.org/licenses/by/4.0/>).